metals

MDPI

Article

Controlled Spintronic Emitter of THz Radiation on an Atomically Thin WS_2/Silicon Substrate

Arseniy Buryakov *, Anastasia Gorbatova, Pavel Avdeev, Nikita Bezvikonnyi, Daniil Abdulaev, Alexey Klimov, Sergei Ovcharenko and Elena Mishina

Laboratory of Femtosecond Optics for Nanotechnology, Department of Nanoelectronics, MIREA—Russian Technological University, 119454 Moscow, Russia
* Correspondence: buryakov@mirea.ru

Abstract: The control and monitoring of the polarization of terahertz radiation are of interest for numerous applications. Here we present a simple controllable THz emitter with a small coercive magnetic field. It is based on a Co/WS_2/silicon structure, in which the presence of uniaxial magnetic anisotropy caused by mechanical stress in a ferromagnetic film was found. Our results show that a ferromagnet/semiconductor emitter can become a technologically simple device for terahertz spintronics.

Keywords: THz emitters; spintronic emitters; THz generation; monolayers; thin films

Citation: Buryakov, A.; Gorbatova, A.; Avdeev, P.; Bezvikonnyi, N.; Abdulaev, D.; Klimov, A.; Ovcharenko, S.; Mishina, E. Controlled Spintronic Emitter of THz Radiation on an Atomically Thin WS_2/Silicon Substrate. *Metals* **2022**, *12*, 1676. https://doi.org/10.3390/met12101676

Academic Editor: Shi-Hoon Choi

Received: 31 August 2022
Accepted: 3 October 2022
Published: 6 October 2022

1. Introduction

The control and monitoring of the polarization of terahertz radiation are of interest for numerous applications. Here, we present a simple controllable THz emitter with a small coercive magnetic field. It is based on a Co/WS_2/silicon structure, in which the presence of uniaxial magnetic anisotropy caused by mechanical stress in a ferromagnetic film was found. Our results show that a ferromagnet/semiconductor emitter can become a technologically simple device for terahertz spintronics. The terahertz range of electromagnetic radiation (0.1–30 THz) has found more and more applications in the last decade, both existing (determining the chemical composition of a substance [1], visualization [2,3] biology [4], medical and pharmaceutical sciences [5]) and being developed (next-generation communication—6G Wi-Fi [6,7]). Such devices require terahertz radiation generators, in which it is possible to control the parameters of the emitted radiation, such as polarization. An example of a source of this type is spintronic emitters. The first spintronic emitter was based on a nanoscale ferromagnet (FM)/non-magnetic (NM) heterostructure. In such an emitter, THz radiation is caused by spin currents generated in the structure under the action of short laser pulses [8]. Depending on the material and the structure, different mechanisms may be responsible for the transformation of the spin current to THz radiation: inverse spin-Hall effect (ISHE) [9–12], Rashba–Edelstein effect (REE) and inverse Rashba–Edelstein effect (IREE) [12,13]. Previously, several ways of controlling polarization in spintronic emitters have been proposed: by simply rotating the magnet around the spintronic structure [14] or by creating a complex magnetic field shape [15]. In the $TbCo_2$/FeCo intermetallic heterostructure with uniaxial magnetic anisotropy, a simple method for controlling the polarization of THz radiation by changing only the current through a magnet was demonstrated [16,17]. In a terahertz emitter deposited on a piezoelectric substrate, the possibility of electrically controlling the polarization of THz wave was shown [18,19].

Another disadvantage of spintronic emitters is their efficiency. This challenge can be solved by using new types of structures. A large number of studies concern new magnetic materials, as well as FM/NM pairs (and heterostructures based on them), but there are works that offer alternative approaches. In [13,20], it was shown that the replacement of a non-magnetic material by a two-dimensional semiconductor (transition metal dichalcogenide TMD) leads to an increase in the efficiency of generation by an order of

magnitude due to the effect of superdiffusion of electrons (electrical spin injection [21]) from a ferromagnet into a semiconductor.

In this work, we investigate spintronic emitters Co (Cobalt)/WS_2. This FM/TMD structure demonstrates a magnetic anisotropy, which provides the manipulation of the polarization of a terahertz wave by changing the magnitude of the magnetic field in both directions of magnetic anisotropy: "easy axis" EA and "hard axis" HA.

2. Materials and Methods

Sample Description and Study Method

We used a commercial sample of WS_2 monolayer on a silicon substrate (Six Carbon Technology Co., Ltd., Shenzhen, China). The sample was grown by a chemical vapor deposition method, has dimensions of 10 × 10 mm and was (100) oriented. WS_2 covers the full area of the substrate. The monolayer ratio is over 95%. A thin film of Co (5 nm) was deposited on WS_2/Si by physical vapor deposition. To protect the magnetic layer from oxidation, a layer of SiO_2 with 3 nm thickness was also deposited on top of the Co layer. The schematic of the sample structure is shown in Figure 1a. The thickness of the layers was additionally confirmed with a variable angle ellipsometer.

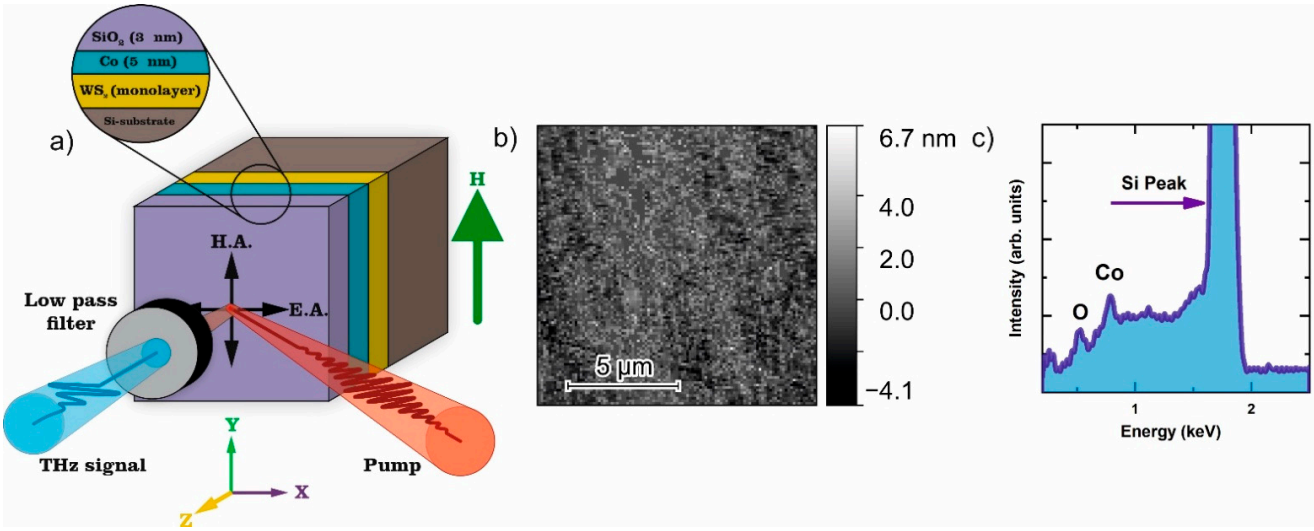

Figure 1. (**a**) Schematic structure of the sample and experimental configuration. (**b**) AFM image of sample surface with a pseudo color scale. (**c**) EDX spectrum characteristic of the sample with 3 peaks correspondent to Co, O, Si. Accelerating voltage is 12 kV.

The structure was examined by atomic force microscopy (AFM) (Figure 1b) and energy dispersive X-ray spectroscopy (EDX) (Figure 1c). From the AFM images of the surface, the root means square roughness was found to be less than ~3 nm along the 30 μm line. An EDX scan was performed with a 12 kV accelerating. The spectrum consists of 3 peaks. A strong peak near 1.8 keV corresponds to Si substrate, ~0.8 keV is the Copeak, ~0.5 keV is the oxygen peak.

3. Results

To study the parameters of the THz radiation generated by the Co/WS_2 heterostructure, we used the THz Time-Domain Spectroscopy (THz-TDS) in the reflection configuration. The choice of such a configuration is due to the high absorption capacity in the terahertz frequency range of the silicon substrate. We irradiated the sample with 35 fs linearly polarized optical laser pulses (800 nm wavelength, 3 kHz repetition rate, diameter 2 mm, 1.7 mJ × cm^{-2}) incident at an angle of 45° to the surface. The emitted THz radiation passing through the THz wire-grid polarizer (WGP) was detected by electro-optical sampling using a ZnTe detector crystal. In this experimental setup, the ZnTe detection system acts as an optical analyzer that measures the *Ex*-component of the THz field. Thus,

in the absence of a THz field, the probe and pump polarizations coincide with the [001] and [−110] axes of the ZnTe crystal, respectively. The [001] axis of the ZnTe coincides with the Y-axis of the laboratory frame (Figure 1a). A detailed description of the optical experiment is presented in the reference [20]. The magnetization direction of Co is controlled by an external magnetic field. The sample was fixed on a non-magnetic holder vertically between two electromagnet cores. Thus, the magnetic field was applied along the Y-axis of the laboratory frame (Figure 1a). A typical time-domain profile of a THz signal generated by the Co/WS_2 heterostructure and corresponding frequency spectra are shown in Figure 2. The maximum spectral amplitude is observed at a frequency of about 0.8 THz, and the frequency bandwidth is limited to 3 THz due to the spectral range of the ZnTe-detector. The THz pulse peak-to-peak signal linearly depends on the fluence of the optical pump (Figure 2b). The terahertz amplitude varies depending on the direction of the applied magnetic field, which confirms the spin-current-based origin of the signal. The efficiency of THz radiation generation in Co/WS_2 is comparable with the efficiency in multilayer $TbCo_2$/FeCo structures reported in our previous works [18,20].

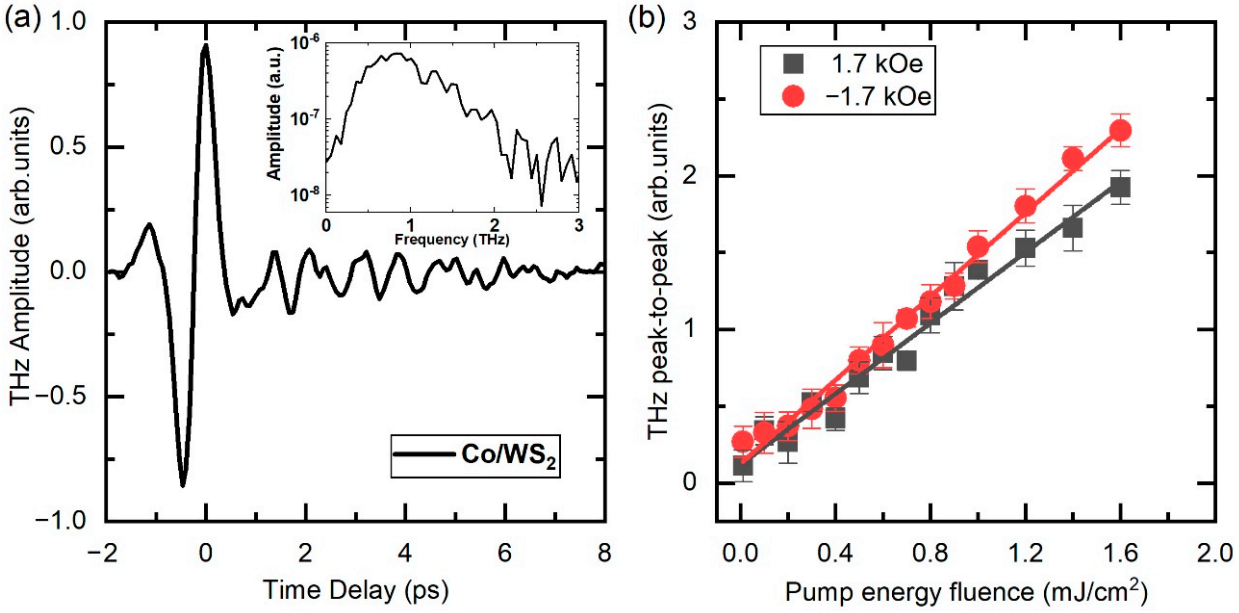

Figure 2. (**a**) Amplitude of terahertz radiation from Co/WS_2 structure in the time and frequency domains (inset). (**b**) THz peak-to-peak amplitude as a function of the pump energy fluence under different magnetic fields applied in the HA geometry.

3.1. THz Signal Hysteresis

The presence of a thin ferromagnetic Co layer leads to the appearance of magnetic properties in the sample and magnetic anisotropy, in particular. Magnetic anisotropy in thin Co layers was demonstrated in [22] and can be described by the Stoner-Wohlfarth model. We associate the occurrence of magnetic anisotropy with the tension of the Co film, which appears due to mechanical stresses between Co and WS_2/Si [23]. The dependencies of the THz signal maximum on magnetic field strength (THz hysteresis loops) are shown in Figure 3a for both the easy and hard axis. Terahertz hysteresis loops were obtained by applying a magnetic field to the emitter, while the THz radiation amplitude was maintained at the maximum point (t = 0 in Figure 2a). The magnetic loops shown in Figure 3a confirm the presence of uniaxial magnetic anisotropy in the sample plane with clearly defined hard and easy axes. In "easy axis" geometry, when a magnetic field is applied in a direction parallel to the easy axis, the THz signal possesses almost a rectangular hysteresis loop with a coercive field of about 0.09 kOe. In "hard axis" geometry, when a magnetic field is applied in a direction orthogonal to the easy axis, the coercive field is about 0.09 kOe. The magnetic hysteresis of the THz amplitude in the Co/WS_2 heterostructure indicates

the rotation of the THz polarization due to the rotation of the magnetic moment in the plane of the sample. The change in the magnetic field strength from negative saturation $-H_s$ towards positive saturation $+H_s$ is accompanied by a change in the THz polarization phase by 180°. Thus, a change in the sign of the magnetizing field inverts the terahertz pulse, which is typical for the spin-based mechanism of THz generation. It is important that the terahertz amplitude rotates together with the direction of the magnetic field, which indicates the spin nature of the generation of THz radiation [24]. The obtained dependences coincide with the corresponding magnetization curves (Figure 3b).

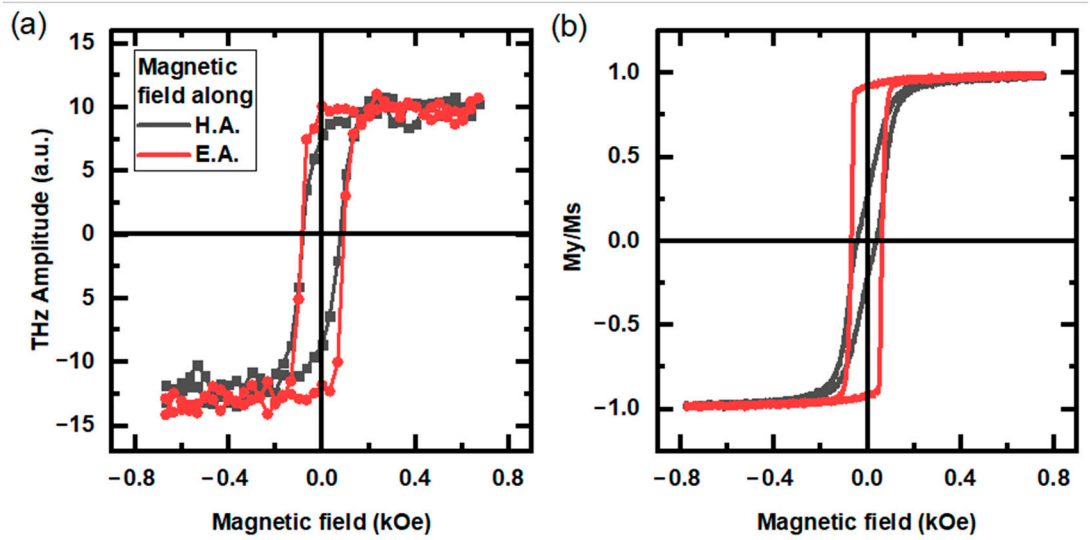

Figure 3. Magnetic hysteresis loops for a Co/WS_2 spintronic emitter for (**a**) a THz signal with an applied magnetic field in the EA and HA; (**b**) magnetization curve.

The Co/WS_2 heterostructure combines three spin mechanisms of THz generation at once: (1) ISHE caused by spin diffusion from FM Co to NM WS_2 under the action of femtosecond laser pulses; (2) IREE caused by the accumulation of spin in the WS_2 monolayer, acting here as a Rashba interface, similar to the work [25]; (3) Ultrafast demagnetization of ferromagnetic layers [26]).

3.2. THz Polarization Rotation

The presence of in-plane magnetic anisotropy in Co/WS_2 (or generally MM/TMD) heterostructures can open up new possibilities for controlled modulation of the THz polarization by an external magnetic field. Magnetization of the sample along the difficult axis would provide a controlled rotation of the THz polarization by changing the current in the magnet (magnetic field magnitude) only. To study the effect of the magnetic field strength on the polarization of THz pulses generated by the Co/WS_2 heterostructure we used the method described in detail in [16]. The experimental dependences of the THz peak-to-peak amplitude on the rotation angle of the THz wire-grid polarizer and the magnetic field in the "hard axis" geometry are shown in Figure 4a (red curves are the best fit to the data). Above each angular dependence (Figure 4a) is a schematic representation of the sample with the laboratory frame, directions of its hard axis, magnetic field, magnetization and polarizations of the optical and THz beams. To fit experimental polarization dependences in the detection scheme with a ZnTe crystal, we used the approach described in Ref. [16], with an additional allowance for the ellipticity of the generated THz wave [27].

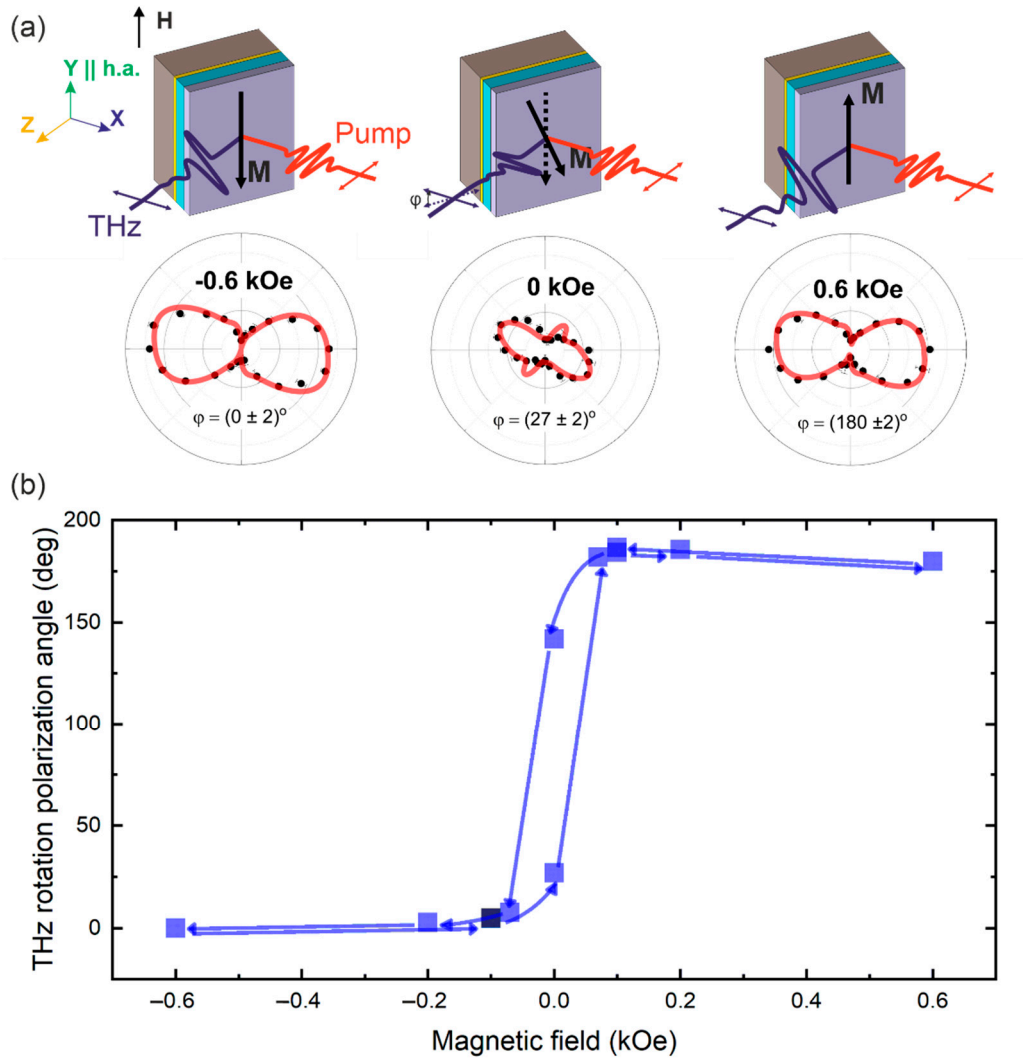

Figure 4. The dependence of the polarization angle of the THz field on the magnetic field in the "hard axis" geometry. (**a**) Angular diagrams of the THz signal (peak-to-peak THz amplitude as a function of the WGP rotation angle—ϕ2) depending on magnetic field. The scale is the same for all angular dependencies. (**b**) Magnetic field dependence of the THz polarization angle obtained from the fittings of angular diagrams.

Figure 4b shows the THz polarization angle as a function of the magnetic field strength in the "hard axis" geometry. Each point on the curve was obtained as a result of the fitting of the THz polarization dependence at the corresponding magnetic field (Figure S1). As can be seen, the curve in Figure 4b fully corresponds to the THz hysteresis loop shown in Figure 3a. Due to the small coercive field and the accompanying sharp change in the phase of the THz signal, the measurement of polarization dependencies in states between the states of positive and negative saturation. Therefore, we can see basically only two polarization states of the THz beam with a phase of 0 and 180°. With a shift from the saturation regions towards 0 kOe, when the residual magnetization is retained in the sample, the maximum polarization rotation is about 30°. Similar results were obtained for the easy axis geometry (Figures S2 and S3). For the easy axis, due to the rectangular form of the THz hysteresis loop, there are only two possible states of the THz polarization. The angular diagrams of the THz polarization for these two states in the region of positive and negative saturation are shown in Figure S3.

3.3. Theoretical Modeling Terahertz Emission

The main problem in describing the processes of generation of THz radiation in spintronic emitters is the difficulty in determining the mechanisms of its occurrence. To date, the main way to separate at least two mechanisms: ISHE and ultrafast demagnetization is carried out experimentally. This is a change in the phase of the THz radiation in the case of sample rotation by 180 degrees for ISHE and no change in the second case (ultrafast demagnetization) [28]. However, this experiment is not always feasible when optically opaque substrates are used. In this paper, we attempt to describe the processes of THz generation using the dependence of THz radiation on the excitation power of the laser pump. We assumed that the main source of THz radiation is the mechanism of ultrafast demagnetization described using the two-temperature model [9]. This model makes it possible to obtain the electron-spin relaxation time, which is presumably equal to the demagnetization time.

The temperature model used describes the distribution of energy (as a result of the action of a laser pulse) between electrons, the crystal lattice and spins. With the help of the temperature model, we can separate the processes between these subsystems.

Using the theoretical model modified for our sample [29], the electron-phonon coupling constant G_{ep} = 7.91 × 10^{17} W × m^{-3} × K^{-1}, the lattice C_p = 3.310^6 J×m^{-3}×K^{-1} electronic C_e = 3.8 × 10^5 J × m^{-3} × K^{-1} heat capacities of the Co ferromagnetic layer.

The electric field emitted by the generator can be defined as [26]:

$$E_x(t) = \frac{\mu_0}{4\pi^2 r}\frac{\partial^2 M_x}{\partial t^2}\left(t - \frac{r}{c}\right) \quad (1)$$

where r—distance to the radiation source. The time dependence of ultrafast demagnetization can be described as follows [30]:

$$M(t) \propto \left\{\Theta(t)\left[A_{es}e^{-\Gamma_{es}t} - A_{ep}e^{-\Gamma_{ep}t}\right]\right\} \otimes G(t), \quad (2)$$

where A_{es} and A_{ep}—amplitudes of electron-spin and electron-phonon scattering, respectively, Γ_{es} и Γ_{ep}—time constants of electron-spin and electron-phonon equilibration respectively, $\Theta(t)$—Heaviside step function, $G(t)$—Gauss function.

A_{es} and A_{ep} were calculated as follows [30]:

$$Aes = \left(\Gamma_{es} - R\Gamma_{ep}\right)/\left(\Gamma_{es} - \Gamma_{ep}\right)$$

$$Aep = (1 - R)\Gamma_{ep}/\left(\Gamma_{es} - \Gamma_{ep}\right) \quad (3)$$

where $R = C_e/C_e + C_p$ and $1/\Gamma_{ep} = G_{ep}/C_e$ = 480 fs.

Further, the experimental results of the generation of THz radiation were approximated by Expression (1) using the previously calculated parameters. Thus, the approximation was carried out with only one fit parameter—Γ_{es}. It should be noted that the use of the calculated value of Γ_{ep} in the approximation did not give satisfactory convergence of the experiment and theory. We attribute this to the fact that the model did not take into account the influence of the nonmagnetic layer WS_2. However, by comparing the results for electron-phonon scattering for pure cobalt with reference to [31], it is clear that our model works precisely for this case. That means that all the differences between this result and the reference for pure cobalt is made up by WS_2 monolayer. Therefore, the value of the parameter Γ_{ep} was obtained from the approximation of the experimental curve for power (160 mW), at which the best convergence of the model and experiment was observed. For the electron-phonon relaxation time, the following value was obtained $\Gamma_{ep} = 1\ ps$. All subsequent experimental curves were approximated with only one fit parameter—Γ_{es}.

Figure 5 shows the values of the electron-spin relaxation times for the dependency of THz radiation on the energy of the exciting pulse. We observe the limit of applicability of the model is limited by the minimum value of the laser radiation energy of 0.6 mJ/cm^2. This may be due to two factors: the simplification of the model (the influence of the nonmagnetic

layer was not taken into account) and the change in the mechanism of generation of THz radiation at the energy of the laser pulse ≥0.6 mJ/cm^2. In favor of the fact that the main contribution to the mechanism of generation of THz radiation is the mechanism of ultrafast demagnetization is indicated by the linear type of dependence of the THz radiation amplitude (Figure 2b) and relaxation time (Figure 5) on the laser radiation energy power.

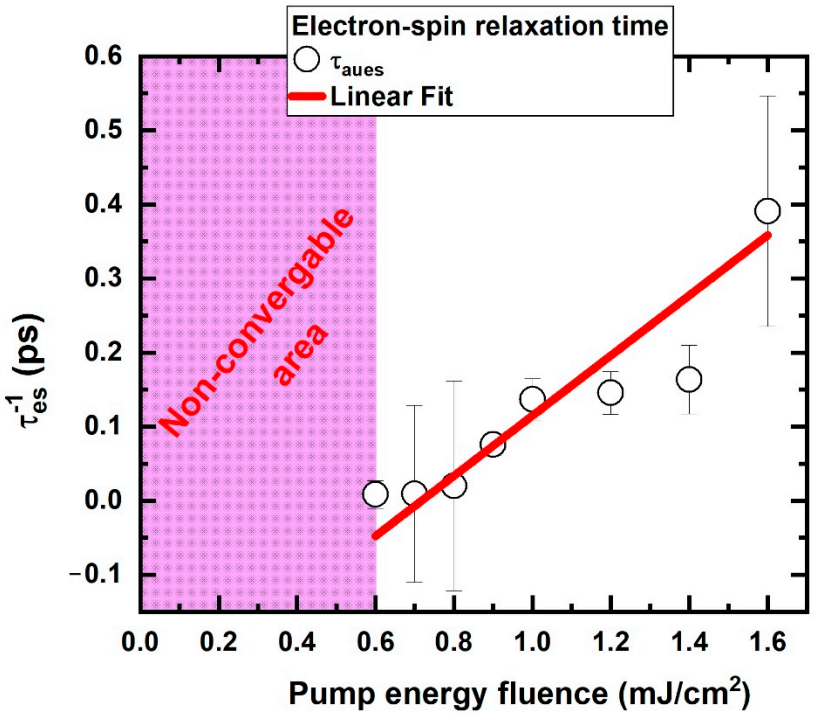

Figure 5. Dependency of the electron-spin relaxation times on the pump energy fluence, obtained from the approximation.

4. Conclusions

In conclusion, a controllable Co/WS_2 THz spintronic emitter with magnetic anisotropy is presented. The total intensity of the THz radiation depends only on the intensity of the optical pump. The rotation of the THz polarization is shown in the range of 0–180° at a record low magnetic field of less than 0.1 kOe. Theoretical modeling has shown that the most probable mechanism of THz radiation in the laser pump energy range 0.6–1.6 mJ/cm^2 is the mechanism of ultrafast demagnetization. The efficiency of the Co/WS_2 emitter is comparable to previously developed controlled THz radiation sources [16,18]. Interestingly, the rather simple design of the device made it possible to create an efficient controllable THz emitter.

Supplementary Materials: The following supporting information can be downloaded at: https://www.mdpi.com/article/10.3390/met12101676/s1, Figure S1: THz hysteresis loop in "hard axis" geometry. Angular dependences of the THz polarization for characteristic points. All characteristic points are marked and numbered on the graph. The scale for all angular dependencies is the same. The rotation angles of the THz polarization for different magnetizing fields found from the approximation are shown on the graph of each angular dependence.; Figure S2: THz hysteresis loop in "easy axis" geometry. Angular dependences of the THz polarization for characteristic points. All characteristic points are marked and numbered on the graph. The scale for all angular dependencies is the same. The rotation angles of the THz polarization for different magnetizing fields found from the approximation are shown on the graph of each angular dependence.; Figure S3: The polarization angle of the THz field as a function of magnetization in the “easy axis” geometry. The scale is the same for both angular dependencies.

Author Contributions: Conceptualization, A.B.; methodology, A.G. and N.B.; software, P.A., N.B. and S.O.; validation, E.M. and A.B.; formal analysis, N.B. and S.O.; investigation, A.G., P.A., A.K. and

N.B.; resources, A.K. and D.A.; data curation, A.B. and A.G.; writing—original draft preparation, N.B., A.G. and A.B.; writing—review and editing, E.M. and A.B.; visualization, N.B., A.G., P.A. and A.B.; supervision, A.B. and E.M.; project administration, E.M. and A.B.; funding acquisition, E.M. All authors have read and agreed to the published version of the manuscript.

Funding: The central part of this work (samples development, fabrication and characterization using all described methods) was supported by the Russian Science Foundation (Grant No. 21-79-10353). The work (characterization basic methods, AFM, EDX) is supported by the Ministry of Education and Science of the Russian Federation (state task No. FSFZ-0706-2020-0022).

Institutional Review Board Statement: Not applicable.

Informed Consent Statement: Not applicable.

Data Availability Statement: The data presented in this study are available on request from the corresponding author.

Conflicts of Interest: The authors declare no conflict of interest.

References

1. Yan, C.; Yang, B.; Yu, Z. Terahertz Time Domain Spectroscopy for the Identification of Two Cellulosic Fibers with Similar Chemical Composition. *Anal. Lett.* **2013**, *46*, 946–958. [CrossRef]
2. Notake, T.; Iyoda, T.; Arikawa, T.; Tanaka, K.; Otani, C.; Minamide, H. Dynamical visualization of anisotropic electromagnetic re-emissions from a single metal micro-helix at THz frequencies. *Sci. Rep.* **2021**, *11*, 1–7. [CrossRef]
3. di Fabrizio, M.; D'Arco, A.; Mou, S.; Palumbo, L.; Petrarca, M.; Lupi, S. Performance Evaluation of a THz Pulsed Imaging System: Point Spread Function, Broadband THz Beam Visualization and Image Reconstruction. *Appl. Sci.* **2021**, *11*, 562. [CrossRef]
4. Bulbul, A.A.M.; Rahaman, H.; Biswas, S.; Hossain, M.B.; al Nahid, A. Design and numerical analysis of a PCF-based bio-sensor for breast cancer cell detection in the THz regime. *Sens. Bio-Sens. Res.* **2020**, *30*, 5419–5430. [CrossRef]
5. Patil, M.R.; Ganorkar, S.B.; Patil, A.S.; Shirkhedkar, A.A. Terahertz Spectroscopy: Encoding the Discovery, Instrumentation, and Applications toward Pharmaceutical Prospectives. *Crit. Rev. Anal. Chem.* **2022**, *52*, 343–355. [CrossRef] [PubMed]
6. Tataria, H.; Shafi, M.; Molisch, A.F.; Dohler, M.; Sjoland, H.; Tufvesson, F. 6G Wireless Systems: Vision, Requirements, Challenges, Insights, and Opportunities. *Proc. IEEE* **2021**, *109*, 1166–1199. [CrossRef]
7. Song, H.J.; Lee, N. Terahertz Communications: Challenges in the Next Decade. *IEEE Trans. Terahertz Sci. Technol.* **2022**, *12*, 105–117. [CrossRef]
8. Seifert, T.; Jaiswal, S.; Martens, U.; Hannegan, J.; Braun, L.; Maldonado, P.; Freimuth, F.; Kronenberg, A.; Henrizi, J.; Radu, I.; et al. Efficient metallic spintronic emitters of ultrabroadband terahertz radiation. *Nat. Photonics* **2016**, *10*, 483–488. [CrossRef]
9. Sasaki, Y.; Takahashi, Y.; Kasai, S. Laser-induced terahertz emission in Co_2MnSi/Pt structure. *Appl. Phys. Express* **2020**, *13*, 093003. [CrossRef]
10. Seifert, T.S.; Tran, N.M.; Gueckstock, O.; Rouzegar, S.M.; Nadvornik, L.; Jaiswal, S.; Jakob, G.; Temnov, V.V.; Münzenberg, M.; Wolf, M.; et al. Terahertz spectroscopy for all-optical spintronic characterization of the spin-Hall-effect metals Pt, W and Cu80Ir20. *Phys. D. Appl. Phys.* **2018**, *51*, 364003. [CrossRef]
11. Ferrolino, J.P.; Cabello, N.I.; de los Reyes, A.; Bardolaza, H.; Verona, I.C.; Mag-Usara, V.K.; Afalla, J.P.; Talara, M.; Kitahara, H.; Garcia, W.; et al. Terahertz spectroscopy for all-optical spintronic characterization of the spin-Hall-effect metals Pt, W and $Cu_{80}Ir_{20}$. *Appl. Phys. Express* **2021**, *14*, 093001. [CrossRef]
12. Cheng, L.; Li, Z.; Zhao, D.; Chia, E.E.M. Studying spin–charge conversion using terahertz pulses. *APL Mater.* **2021**, *9*, 070902. [CrossRef]
13. Cheng, L.; Wang, X.; Yang, W.; Chai, J.; Yang, M.; Chen, M.; Wu, Y.; Chen, X.; Chi, D.; Goh, K.E.J.; et al. Far out-of-equilibrium spin populations trigger giant spin injection into atomically thin MoS2. *Nat. Phys.* **2019**, *15*, 347–351. [CrossRef]
14. Kong, D.; Wu, X.; Wang, B.; Nie, T.; Xiao, M.; Pandey, C.; Gao, Y.; Wen, L.; Zhao, W.; Ruan, C.; et al. Broadband Spintronic Terahertz Emitter with Magnetic-Field Manipulated Polarizations. *Adv. Opt. Mater.* **2019**, *7*, 1900487. [CrossRef]
15. Chen, X.; Wu, X.; Shan, S.; Guo, F.; Kong, D.; Wang, C.; Nie, T.; Pandey, C.; Wen, L.; Zhao, W.; et al. Generation and manipulation of chiral broadband terahertz waves from cascade spintronic terahertz emitters. *Appl. Phys. Lett.* **2019**, *115*, 221104. [CrossRef]
16. Khusyainov, D.; Ovcharenko, S.; Gaponov, M.; Buryakov, A.; Klimov, A.; Tiercelin, N.; Pernod, P.; Nozdrin, V.; Mishina, E.; Sigov, A.; et al. Polarization control of THz emission using spin-reorientation transition in spintronic heterostructure. *Sci. Rep.* **2021**, *11*, 1–8. [CrossRef]
17. Koleják, P.; Lezier, G.; Postava, K.; Lampin, J.-F.; Tiercelin, N.; Vanwolleghem, M. 360° Polarization Control of Terahertz Spintronic Emitters Using Uniaxial FeCo/$TbCo_2$/FeCo Trilayers. *ACS Photonics.* **2021**, *9*, 1274–1285. [CrossRef]
18. Khusyainov, D.; Ovcharenko, S.; Buryakov, A.; Klimov, A.; Pernod, P.; Nozdrin, V.; Mishina, E.; Sigov, A.; Preobrazhensky, V.; Tiercelin, N. Composite Multiferroic Terahertz Emitter: Polarization Control via an Electric Field. *Phys. Rev. Appl.* **2022**, *17*, 044025. [CrossRef]

19. Lezier, G.; Koleják, P.; Lampin, J.-F.; Postava, K.; Vanwolleghem, M.; Tiercelin, N. Fully reversible magnetoelectric voltage controlled THz polarization rotation in magnetostrictive spintronic emitters on PMN-PT. *Appl. Phys. Lett.* **2022**, *120*, 152404. [CrossRef]
20. Khusyainov, D.; Guskov, A.; Ovcharenko, S.; Tiercelin, N.; Preobrazhensky, V.; Buryakov, A.; Sigov, A.; Mishina, E. Increasing the Efficiency of a Spintronic THz Emitter Based on WSe_2/FeCo. *Materials* **2021**, *14*, 6479. [CrossRef]
21. Battiato, M.; Held, K. Ultrafast and Gigantic Spin Injection in Semiconductors. *Phys. Rev. Lett.* **2016**, *116*, 196601. [CrossRef] [PubMed]
22. Chappert, C.; Bruno, P. Magnetic anisotropy in metallic ultrathin films and related experiments on cobalt films. *J. Appl. Phys.* **1988**, *64*, 5736–5741. [CrossRef]
23. Demidov, V.V.; Borisenko, I.V.; Klimov, A.A.; Ovsyannikov, G.A.; Petrzhik, A.M.; Nikitov, S.A. Magnetic anisotropy of strained epitaxial manganite films. *Exp. Theor. Phys.* **2011**, *112*, 825–832. [CrossRef]
24. Huisman, T.J.; Mikhaylovskiy, R.V.; Costa, J.D.; Freimuth, F.; Paz, E.; Ventura, J.; Freitas, P.P.; Blügel, S.; Mokrousov, Y.; Rasing, T.; et al. Femtosecond control of electric currents in metallic ferromagnetic heterostructures. *Nat. Nanotechnol.* **2016**, *115*, 455–458. [CrossRef]
25. Zhou, C.; Liu, Y.P.; Wang, Z.; Ma, S.J.; Jia, M.W.; Wu, R.Q.; Zhou, L.; Zhang, W.; Liu, M.K.; Wu, Y.Z.; et al. Broadband Terahertz Generation via the Interface Inverse Rashba-Edelstein Effect. *Phys. Rev. Lett.* **2018**, *121*, 086801. [CrossRef] [PubMed]
26. Beaurepaire, E.; Turner, G.M.; Harrel, S.M.; Beard, M.C.; Bigot, J.-Y.; Schmuttenmaer, C.A. Coherent terahertz emission from ferromagnetic films excited by femtosecond laser pulses. *Appl. Phys. Lett.* **2004**, *84*, 3465–3467. [CrossRef]
27. Khusyainov, D.I.; Gorbatova, A.V.; Buryakov, A.M. Terahertz generation from surface of the bulk and monolayer tungsten diselenide. *Russ. Technol. J.* **2020**, *8*, 121–129. [CrossRef]
28. Wang, X.; Cheng, L.; Zhu, D.; Wu, Y.; Chen, M.; Wang, Y.; Zhao, D.; Boothroyd, C.B.; Lam, Y.M.; Zhu, J.; et al. Ultrafast Spin-to-Charge Conversion at the Surface of Topological Insulator Thin Films. *Adv. Mater.* **2018**, *30*, 1802356. [CrossRef]
29. Hargreaves, R. Ultrafast Demagnetisation as a Terahertz Source, Master of Science. Master's Thesis, School of Physics, University of Wollongong, 2014. Available online: https://ro.uow.edu.au/theses/4274 (accessed on 2 October 2022).
30. Rouzegar, R.; Brandt, L.; Nadvornik, L.; Reiss, D.A.; Chekhov, A.L.; Gueckstock, O.; In, C.; Wolf, M.; Seifert, T.S.; Brouwer, P.W.; et al. Laser-induced terahertz spin transport in magnetic nanostructures arises from the same force as ultrafast demagnetization. *arXiv* **2021**, arXiv:2103.11710.
31. Labort-Ibarre, A.; Voisin, C.; Cassabois, G.; Delalande, C.; Flytzanis, C.; Roussignol, P.; Beauvillain, P. Ultrafast electron thermalization in a magnetic layered Au/Co/Au film. *J. Appl. Phys.* **2008**, *104*, 094301. [CrossRef]